Transformations between tetrahedrally and octahedrally coordinated crystals: the wurtzite → rocksalt and blende → rocksalt mechanisms

2002 J. Phys.: Condens. Matter 14 4629

(http://iopscience.iop.org/0953-8984/14/18/301)

INSTITUTE OF PHYSICS PUBLISHING JOURNAL OF PHYSICS: CONDENSED MATTER

J. Phys.: Condens. Matter **14** (2002) 4629–4643 PII: S0953-8984(02)33898-0

Transformations between tetrahedrally and octahedrally coordinated crystals: the wurtzite → rocksalt and blende → rocksalt mechanisms

Mark Wilson[1] **and Paul A Madden**[2]

[1] Department of Chemistry, University College London, 20 Gordon Street, London WC1H 0AJ, UK
[2] Physical and Theoretical Chemistry Laboratory, Oxford University, South Parks Road, Oxford OX1 3QZ, UK

Received 18 February 2002
Published 26 April 2002
Online at stacks.iop.org/JPhysCM/14/4629

Abstract

The mechanism of the pressure-driven phase transformation from the wurtzite (B4) to rocksalt (B1) crystal structures is studied in a 'constant-stress' molecular dynamics simulation of a model ionic system. The mechanism differs significantly from that exhibited by the same system in transforming from the zinc blende structure (B3) to rocksalt, despite the fact that the B3 and B4 phases differ only in their stacking sequences. This is traced to the difference between the crystal structures at the next-nearest-neighbour level and discussed in terms of the preponderance of boat and chair six-membered rings within the two structures. The relationship between the observed mechanism and those which have been proposed on the basis of crystallographic studies is explored. In particular the way in which the stability of potential intermediate phases is influenced by the interatomic interactions is discussed.

(Some figures in this article are in colour only in the electronic version)

1. Introduction

A large number of systems of MX stoichiometry undergo a transition from the four-coordinate cubic blende (B3) or hexagonal wurtzite (B4) structures to the six-coordinate rocksalt (B1) on the application of moderate pressures. The B3 and B4 structures are closely related. In both cases, the anions adopt a close-packed arrangement in which the cations occupy one-half of the available tetrahedral holes. From this viewpoint, the structures differ only in the stacking sequences adopted by successive ion layers [1]. As illustrated in figure 1, in the B3 the sub-lattices adopt a cubic-close-packed ABCABC... sequence, whilst in the B4 the ions adopt the hexagonal-close-packed ABABAB... arrangement. In the rocksalt structure the

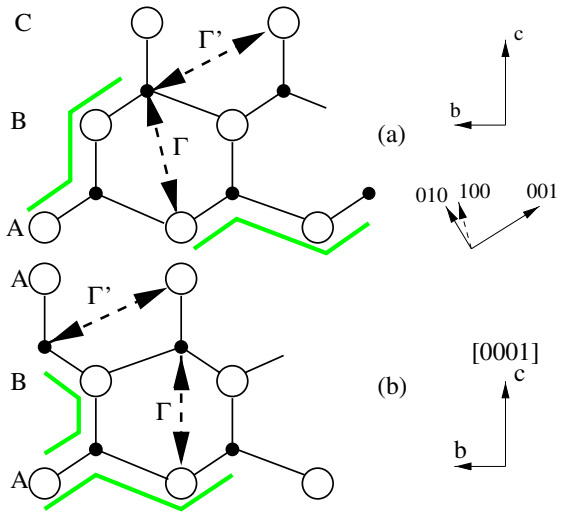

Figure 1. Schematic representation of the B3 (blende) and B4 (wurtzite) structures shown with the close-packed planes horizontal so that the different stacking sequences—B3 ABC... stacking, B4 ABA...—are apparent. In the B3 the close-packed planes are perpendicular to the [111] directions of the normal cubic unit cell, whereas in the hexagonal wurtzite structure they form the basal planes, perpendicular to [0001] of the hexagonal cell. The next-nearest-neighbour distances, Γ and Γ', are highlighted (these are equivalent in the B3 structure). The light thick lines illustrate the 'chairs' and 'boats' of six-membered rings discussed in the text. In the simulations these structures will be set up in hexagonal cells with the c-axis vertical and the a-axis coming out of the plane, and the b-axis making an angle of 120° to it.

sublattices are cubically close packed and the ions of one type occupy the *octahedral* holes of the other sublattice. The difference in hole occupancy makes it clear that the mechanism of the transition cannot be simply martensitic; 'bonds' must be broken and/or formed in the course of the transformation. Furthermore, since such bond reorganizations will be affected by the chemistry of the elements involved, it is likely that the mechanism will depend on the material involved, though the range of possible mechanisms will be limited by the symmetries of the allowed pathways between the two crystal structures [2].

To understand the nature of these mechanisms has become a matter of practical significance since many II–VI and III–V semiconductors adopt the blende or wurtzite structure in their crystalline ground state. There is much interest in controlled synthesis of nanostructures of these materials [3] and such processes could be affected by the proximity of the six-coordinate phase. Alivisatos and co-workers [3] have already demonstrated substantial particle size effects on the thermodynamics and kinetics of the pressure-driven phase transition and have pointed out major changes in particle shape in the course of the transformation. Starting with a nanocrystal of a particular habit, the mechanism will determine which crystal faces of the product (or any intermediate) phase are exposed during the transformation and hence influence surface contributions to the free energy barrier controlling the kinetics. In the B3 → B1 or B4 → B1 transformations, surface effects could be very large if polar surfaces were exposed.

Given the close relationship of the B3 and B4 structures (viewed as interpenetrating, close-packed sublattices), one might imagine that very similar mechanisms would occur in their transitions to the B1 structure. However, as we show in detail below, this is not the case. We have previously examined [4] the mechanism for the B3 → B1 transition for a model ionic system ('MCl') in molecular dynamics simulations. The use of such methods, on sufficiently large

length and timescales, allows the system to find its own pathway between the two structures, and the mechanism identified by examining the atomic trajectories. Besides doing this for MCl itself, we were able to characterize possible intermediate crystalline phases, such as litharge or d-β-Sn, which have sometimes been invoked in crystallographic studies of phase transitions from the blende structure (see, for example, [5–8] for reviews), and therefore to discuss how chemical factors would influence the transition pathway for other materials. The mechanism we identified for the B3 $\rightarrow$ B1 of MCl consisted of an initial tetragonal distortion of the cubic unit cell, associated with a specific deformation of the tetrahedral shell around each cation, followed by a concerted glide of planes perpendicular to the 100 direction [4]. This mechanism is readily described as a deformation (and subsequent reconstruction) of a cubic cell, which is the natural cell to describe the blende structure. We now find (see below) that the B4 $\rightarrow$ B1 transition in MCl cannot be described in the same terms; indeed, one can see that the same type of rearrangement would be blocked by the lower symmetry inherent in the hexagonal structure.

An alternative viewpoint to that of close-packed lattices, which provides a better basis for understanding this difference of mechanisms, is to consider the topology of the anion–cation bonds (a 'bond' being defined as connecting a nearest-neighbour anion–cation pair). In these terms, the B3 and B4 structures can be considered as constructed from an infinite three-dimensional network of wholly corner-sharing MX_4 (or XM_4) tetrahedra. The difference between the two structures now lies in the way in which these tetrahedra link together. As illustrated in figure 1, if we consider a single MX_4 tetrahedron, then the next such unit in the vertical direction can have one of two orientations whilst retaining the imposed bond angles. If this second tetrahedron is in the same orientation as the first, then the third anion layer will not lie above the first, and this corresponds to the cubic-packed B3 lattice. Alternatively, if the second tetrahedron is oriented at 180° with respect to the first, then the third anion layer will lie directly on top of the first giving the hexagonally packed B4 structure. In both cases, only six-membered rings (consisting of three MX molecules) are formed. In both structures the rings in the horizontal plane are exclusively in a 'chair' configuration (as highlighted in figure 1). The difference arises perpendicular to this. In the B3 structure, all of these rings are also chairs whilst in the B4, the rings are in 'boat' configurations. As a result, the B4 and B3 structures differ at the next-nearest-neighbour anion–cation level. As shown in figure 1, these (Γ and Γ') are equivalent in the B3 structure but may be different in the B4 (with $\Gamma < \Gamma'$). Relaxation of these distances may allow the wurtzite structure to achieve a lower energy than the blende, leading to a c/a ratio (figure 1) which differs from the ideal hexagonal close-packed value of 1.633. However, as we shall show, when the crystals are squeezed by an imposed pressure, the different response of the boats and chairs blocks the pattern of atomic displacements responsible for the transition seen in the blende structure.

The B4 $\rightarrow$ B1 transformation has been studied experimentally by applying both gradual pressure (in CdSe [9]) and shocking the crystals by the rapid application of pressure (in CdS [10–12]). In the case of the shock experiments, a relatively simple reaction pathway is proposed via a two-step process with a stable intermediate structure (termed the face-centred tetragonal—fct). *Ab initio* calculations on CdS at selected points along the proposed transition pathway have been interpreted as supporting this proposal [12]. Further *ab initio* calculations have been performed on MgO and GaN in which an alternative hexagonal (h-MgO) intermediate is proposed [13, 14]. In addition, recent work has focused on studying the transformation in CdSe nanocrystallites [3].

In this paper we follow the same strategy as in our earlier study of the B3 $\rightarrow$ B1 transition; we allow the system to find its own pathway in a 'constant-stress' molecular dynamics simulation in which the isotropic pressure is continuously increased. We use the same interionic potential as in the earlier paper. In order to compare the B3 and B4 mechanisms

Table 1. Thermodynamic and pressure data for the four transitions studied. ΔU is the energy difference at the volume minimum with respect to the lowest-energy (B4) phase. P_t is the static (0 K) phase transition pressure taken from the tangents of the energy/volume curves. P_t' is the dynamic pressure range over which the transformation proceeds during the constant-stress molecular dynamics. ΔV is the volume change on transition. ΔG^{over} is the energy associated with the overpressure $P_t' - P_t$.

System	ΔU (kJ mol^{-1})	P_t(0 K)	P_t' ($\Longrightarrow$)	$\Delta V\%$	ΔG^{over}
B3 $\rightarrow$ B1	2.0	4.8	15.0–21.0	11.3	19
B4 $\rightarrow$ B1	—	5.7	26.6–29.4	9.0	26
B5 $\rightarrow$ B1	1.3	5.1	17.8–21.9	12.5	23
SF $\rightarrow$ B1	0.7	5.4	20.9–26.2	11.4	27

we set up all the initial configurations in hexagonal simulation cells, so that the a and b sides of the cell lie in the horizontal close-packed planes of figure 1 and the c side is vertical. We begin by comparing the transitions from different starting structures at the 'macroscopic' level—examining the transition pressures and the behaviour of the unit cell parameters. We then review the mechanism we established for the B3 $\rightarrow$ B1 transition in the first paper (studied there in the normal cubic cell) from this hexagonal cell perspective and contrast this with that found from the B4 starting point. As stressed at the outset, the B3 and B4 structures have different stacking sequences (ABC... and ABAB...); it is possible also to set up an intermediate stacking sequence, like ABACABAC (B5), and see how this tips the balance towards the B3 or B4 mechanism, and we pursue this as a way of confirming our analysis of the origin of the different mechanisms. Finally we compare our proposed mechanism for the B4 $\rightarrow$ B1 transition with those which have been proposed from experimental studies, highlighting the potential role of intermediate phases.

2. Macroscopic effects

The present work is directed towards understanding the difference between the B3 $\rightarrow$ B1 and B4 $\rightarrow$ B1 transitions in the model ionic system 'MCl', for which the potential is described in [4]. As shown by the internal energy versus volume (U/V) curves for the fully relaxed crystal structures in figure 2, the MCl potential has a ground-state crystal structure which is B4, with the B3 at slightly higher energy (2 kJ mol^{-1}) and very similar molar volume. Its optimum c/a ratio is 1.59, compared with the ideal (hexagonal close-packed) value of 1.633. These four-coordinate structures exhibit transitions to the denser, six-coordinate rocksalt structure at an equilibrium transition pressure of about 5 GPa (as estimated from a common tangent to the U/V curves). Since we envisage the close-packed layer nature of the stacking sequence to be a significant factor in the transformation mechanism, we shall consider two further transformations on stacking sequences which can be considered as intermediate between the B3 and B4. In the first (the B5 structure) the stacking sequence is ABACABAC... . In the second case we focus on a B4 cell which contains two simple stacking faults (referred to as SF) [15] giving an ABABACBCBC... stacking sequence. As shown in figure 2 their energy/volume curves lie intermediate between the B4 and B3. Equilibrium transition pressures to the B1 crystal, from each of these four-coordinate structures, are given in table 1.

The phase transition is driven by a steady increase in the isotropic pressure in the constant-stress simulations, as described in [4]. Physical factors controlling the rate at which the pressure can be increased were discussed in [4], and we use the same rates in the present work (see appendix for details of the simulation cells and other parameters controlling the simulations).

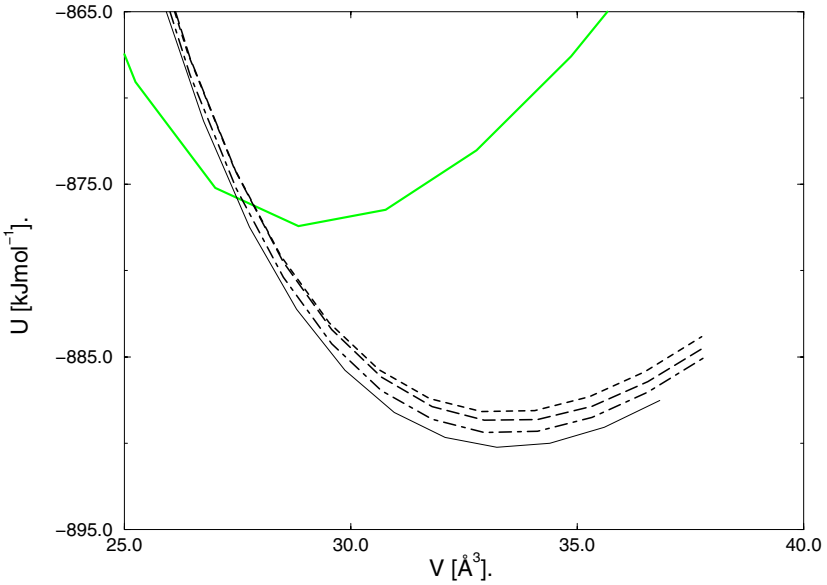

Figure 2. Energy/volume curves for the octahedral B1 (high-pressure) phase and the four fully relaxed tetrahedral phases considered here. Key: solid curve—B4, dashed curve—B3, long-dashed curve—B5, dot–dashed curve—SF, thick light curve—B1.

Figure 3 shows the variation of the c/a ratio as the pressure is progressively increased in the course of the MD run for the four transitions. To aid direct comparison all of the c/a ratios have been 'normalized' to the ideal B4 value. The rapid changes in each curve above 10 GPa are indicative of the onset of the phase transition itself. Until this point is reached, the B3 c/a ratio remains rigidly at the ideal value reflecting the equivalence of Γ and Γ' in figure 1. The B4 c/a ratio shows a near-linear decrease with increasing pressure with both the B5 and SF structures showing the same effect, but to a lesser degree. In these three systems the next-nearest-neighbour anion–cation length, Γ, becomes compressed by the application of pressure, to a greater degree than Γ'. The transformation from the ideal blende (B3) structure to the B1 shows the lowest pressure transformation whilst the change from the ideal wurtzite (B4) requires the highest pressure. These driving pressures are listed in table 1. The pressures required to drive these respective transitions dynamically are greater than the ideal static transition pressures. These overpressures can be written in terms of a thermodynamic driving force,

$$\Delta G(p) = \Delta V(p - p_t), \tag{1}$$

where p is the dynamic transformation pressure, p_t is the ideal static transition pressure and ΔV is the volume change on transformation (and is taken as constant over the pressure range for each transition). These energies are listed in table 1. The energy associated with driving the B3 transition appears significantly smaller than those required to drive the other three systems (which all contain elements of hexagonal close-packing).

3. Mechanism of the B3 → B1 transition revisited

We begin with a reconsideration of the B3 → B1 transition in an initially hexagonal cell, where the crystallographic [111] direction of the B3 structure lies along the c-direction. In the previous

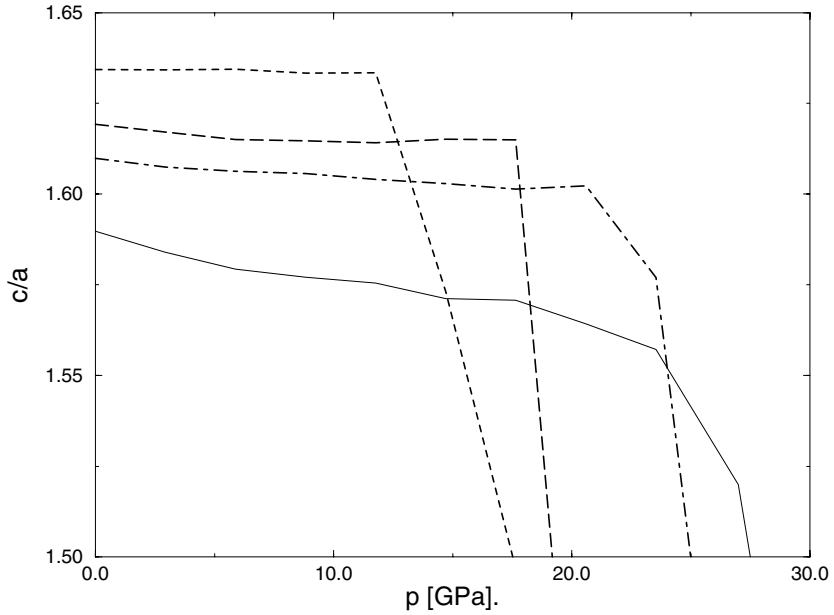

Figure 3. Variation of the B4, B3, B5 and SF c/a ratio with pressure observed in the course of the pressure ramped MD runs. The abrupt change marks the onset of the phase transition. Key: solid curve—B4, dashed curve—B3, long-dashed curve—B5, dot–dashed curve—SF.

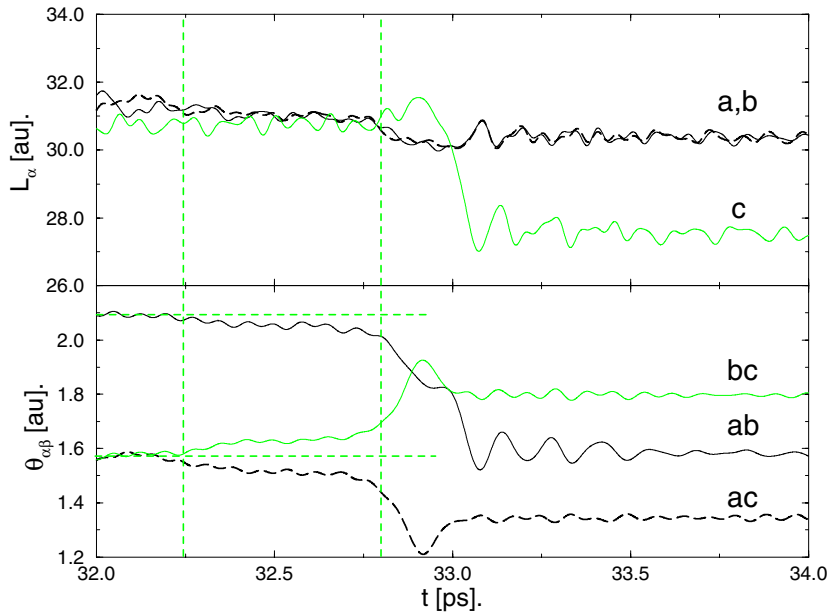

Figure 4. Time evolution of the cell lengths (upper panel) and cell angles (lower) for the B3 $\rightarrow$ B1 phase transition. The vertical dashed lines indicate the (approximate) times at which significant changes take place in the cell angles and/or lengths. The horizontal dashed curves in the lower panel are drawn to highlight the subtle early changes in angles.

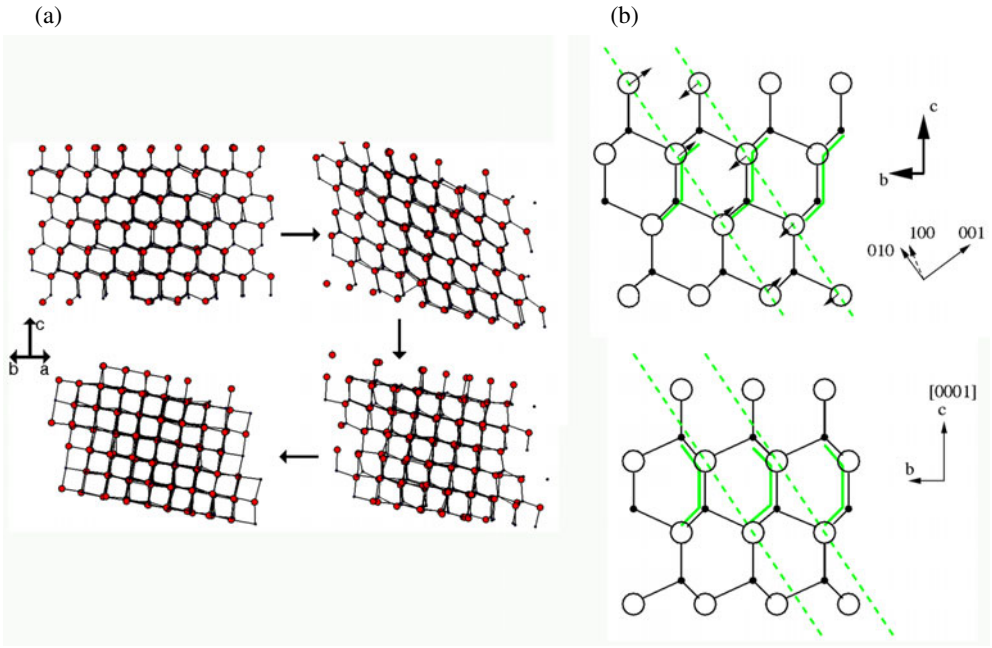

Figure 5. (*a*) Molecular graphics snapshots of the B3 crystal as it goes through the pressure-driven phase transition. From top left and going clockwise: at 32.0, 32.5, 32.9 and 33.2 ps. (*b*) The upper panel shows the B3 structure viewed as indicated. The light dashed lines indicate the planes of anions that compress (as indicated by the arrows) to form the d-β-Sn transition structure. The lower panel, for the B4 structure, shows that analogous planes of deformable tetrahedra do not occur in this crystal. The chairs and boats perpendicular to the ab-plane are highlighted by the light thick lines.

study of B3 we used a cubic simulation cell, whose edges coincided with the [100] directions. Apart from allowing us to visualize the transformation from the same reference frame as naturally used for the B4, this is a useful check on the simulation algorithm [16] and the way it has been implemented in our code, since the results should be independent of the choice of simulation cell [17].

In the previous study [4] the transformation was seen to occur in two steps. Initially, the three equivalent cell lengths in the cubic simulation cell decouple, with two lengths increasing whilst the third length decreases, corresponding to an initial tetragonal distortion of the B3 unit cells. *Subsequently* there is a shearing motion of the lattice; two of the cell angles remain at 90°, whilst a third goes to ∼110°. As a result of this transformation, the orientation of the close-packed anion sublattice changes, with a $\langle 100 \rangle_{B3}$ lattice vector becoming the $[111]_{B1}$ of the final structure. The applied pressure range over which the transition was observed was 15–21 GPa.

In figure 4 we show the time evolution of the cell lengths and angles over the portion of the MD run where the system transforms to the B1. The most significant changes in both cell lengths and angles occur at ∼32.8 ps (indicated by a line in the figure). At this time, the a and b cell lengths are reduced by around 3% with a much larger reduction in the c-direction length (∼10%). As these lengths evolve there are corresponding changes in the cell angles, with the $\widehat{ab}$-, $\widehat{ac}$- and $\widehat{bc}$-angles changing to 91°, 77° and 103° respectively. It is noticeable, however, that significant changes in the cell angles occur at around 32.25 ps (again indicated

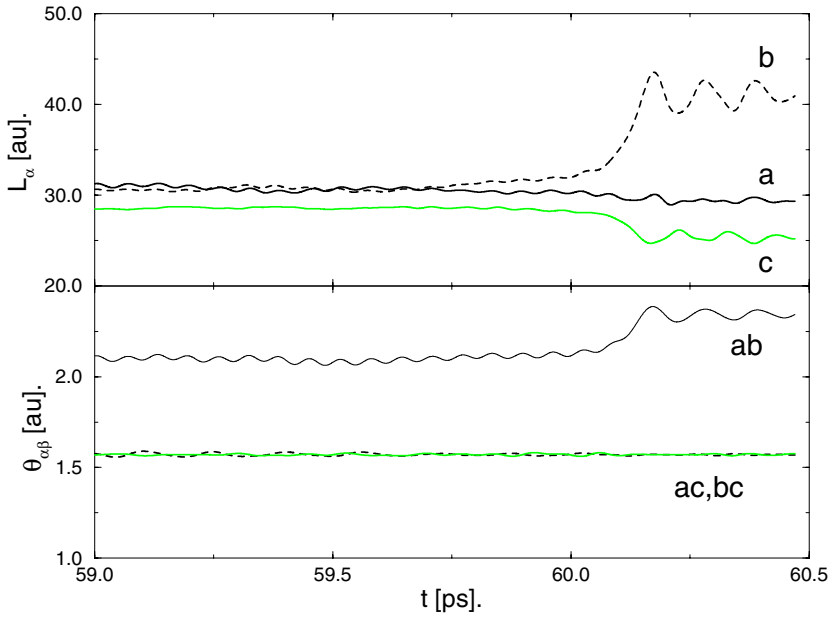

Figure 6. Time evolution of the cell lengths (upper panel) and cell angles (lower) for the B4 → B1 phase transition. Note that the changes in these parameters appear to coincide, in contrast to the B3 case.

by a line in the figure). The $\widehat{ac}$- and $\widehat{bc}$-angles, originally 90°, are split, becoming 86° and 94° respectively, with a corresponding reduction in the $\widehat{ab}$ cell angle from 120° to 116°. This two-stage nature of the transition and the values of the transition pressure and volume are wholly consistent with our previous observations in the cubic cell. We now consider the pattern of atomic displacements from the hexagonal cell perspective.

Figure 5(*a*) shows four molecular graphics 'snapshots' of the B3 simulation cell as it passes through the phase transition, viewed along a line perpendicular to the *c*-direction and bisecting the *a*- and *b*-directions (which is equivalent to the schematic projection of the B3 structure shown in figure 1). Panel (i) (top left) shows the ion positions at 32.0 ps, that is, prior to the onset of the phase transition as indicated by the changes in both cell lengths and angles indicated in figure 4. Panel (ii) shows the ion positions at 32.5 ps (i.e. in the middle of the two-stage change in the cell parameters) in which the tetrahedra have become compressed. This is analogous to the cubic to tetragonal distortion observed for the B3 transition starting from a cubic cell [4], and characteristic of a distortion towards a d-β-Sn structure. This compression corresponds to the subtle changes in the cell angles which begin at ∼32.25 ps in figure 4. In the third panel (corresponding to 32.85 ps) the second-stage shearing motion is in progress with the cations moving away from the tetrahedral sites so as to form octahedral sites. In the final panel (bottom left, at ∼33.2 ps) the final B1 crystal structure has been formed.

To clarify the nature of the ionic displacements observed during the phase transition, figure 5(*b*) shows an idealized stacking sequence for the B3 crystal (upper panel), displayed in the same orientation as in figure 1 and an equivalent orientation to figure 5(*a*), compared with the B4 (lower panel). In the pattern identified previously [4], the first step is a tetragonal distortion to the d-β-Sn in which two adjacent planes of MX_4 tetrahedra are compressed, as indicated by the arrows. The light dashed lines highlight the planes which compress together

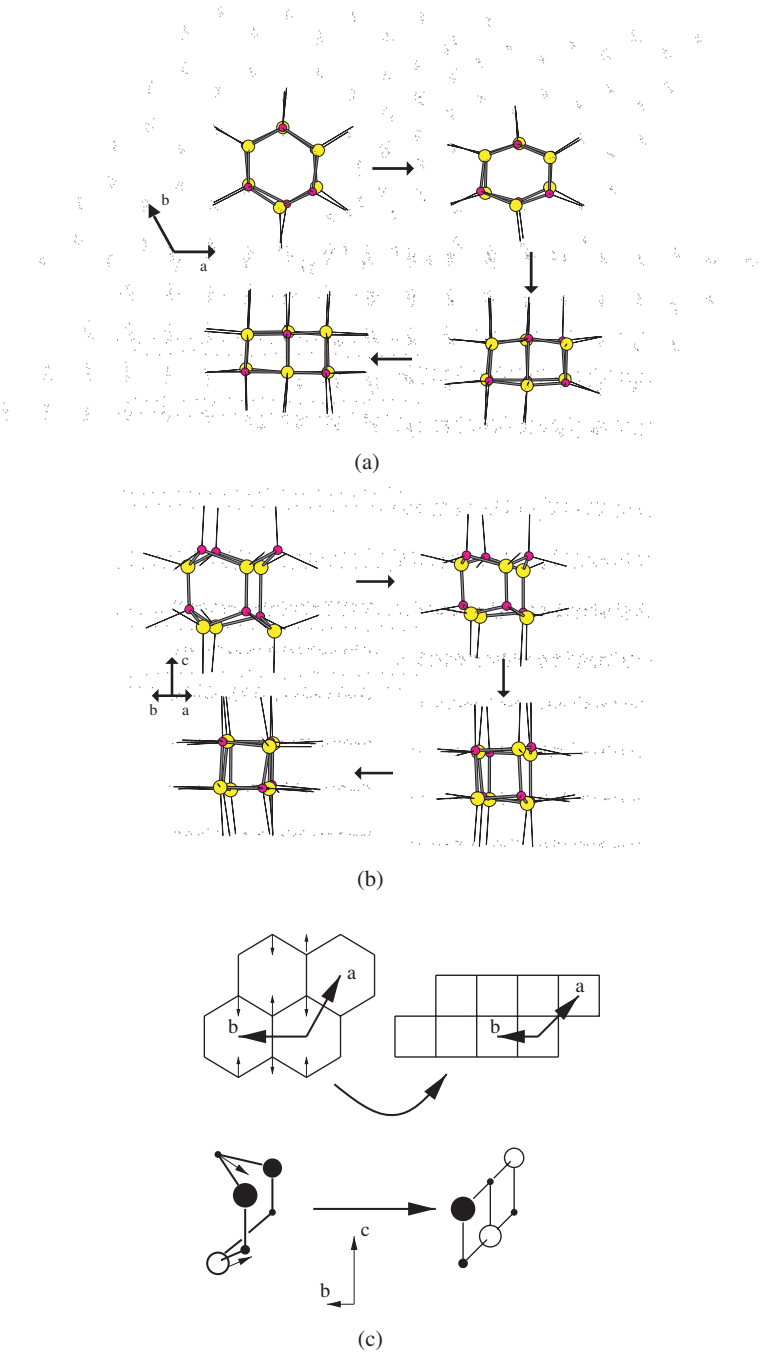

Figure 7. Molecular graphics snapshots of the B4 crystal as it undergoes the pressure-driven phase transition (from top left going clockwise). The crystal is viewed (*a*) in the *ab*-plane, (*b*) in a plane perpendicular to the *ab*, as indicated by the axes. (*c*) Schematic representation of the B4 $\rightarrow$ B1 transformation mechanism. The upper panel shows the [*ab*] basal plane with the arrows indicating the distortion to form the 3 $\times$ 2 B1 face units. The lower panel shows one of the boats in the *c*-direction collapsing to the 3 $\times$ 2 square net.

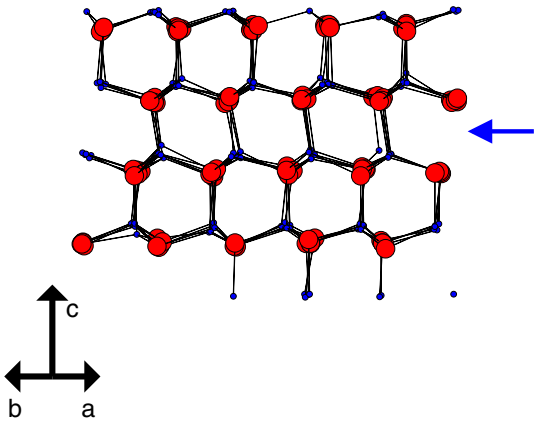

Figure 8. A molecular dynamics snapshot of the B5 structure viewed down the $[10\bar{1}0]$-axis prior to the pressure-driven phase transition. The arrow indicates the strained layer of chair structures.

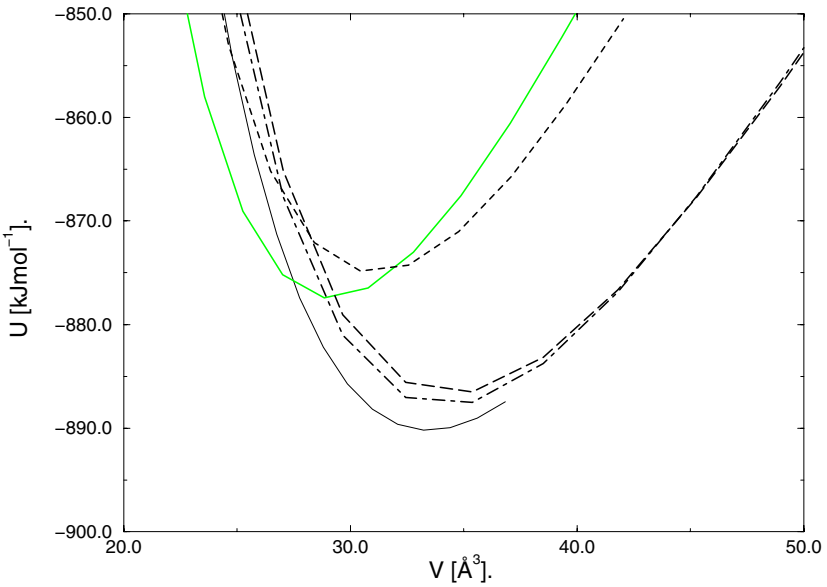

Figure 9. Energy/volume curves for the two potential intermediates. Key: solid line—B4, light solid curve—B1, dashed curve—fct, long-dashed curve—h-MgO ($u = 0.50$), dot–dashed curve—h-MgO ($u = 0.45$).

to form the d-β-Sn transition structure. The result of this compression is that two pairs of next-nearest-neighbour anions are moved closer to a given cation. In the second stage, the cations move in order to form a new octahedral hole using two of these four next-nearest neighbours, along with its original four neighbours, to form the local octahedral coordination polyhedron.

The lower panel of the figure shows, schematically, an analogous four-anion layer section for the B4 structure. As is clear from the figure, analogous planes of distorted tetrahedra cannot be constructed for the B4 structure. In terms of the chair and boat terminology, one can say that it is the presence of the boat structures in the c-direction for the B4 structure which does not allow for the formation of the same layers as in the B3 structure. As a result, the potential

distortion to a d-β-Sn-like structure is not an option for the B4 structure without additional ion motions and so, as we shall see below, an alternative mechanistic pathway is selected.

4. B4 → B1

Figure 6 shows the time evolution of the cell lengths and angles for the simulation of the B4 → B1 transition at 300 K, starting from an equilibrated zero-pressure ideal wurtzite crystal, over the narrow time domain in which the transition occurs. In contrast to the B3 → B1 transition, the cell lengths and angles appear to transform simultaneously, with the $\widehat{ab}$-angle increasing from 120° to 135°. The cell length in the b-direction increases by around 34% with simultaneous smaller reductions in both the a- and c-directions. The volume change at the transition pressure is around 9% (see table 1). The mean bond lengths increase from around 2.02 to 2.20 Å consistent with an increase in ion coordination number.

Examination of the pattern of atomic displacements shows that the transformation mechanism is consistent with those proposed previously from experimental observations [9–12], as we shall discuss in more detail below. Figures 7(a) and (b) show a series of molecular graphics snapshots taken as the B4 system goes through the phase transition, looking at the ab-and ac-planes respectively. The latter projection is equivalent to that idealized in figure 1. Figure 7(c) shows a schematic representation of the motion of the ions in the same two planes. In the ab-plane (figure 7(a) and the upper panel of figure 7(c)), a hexagon of three MX molecules in a chair conformation distorts so as to form a planar pattern of 3 × 2 rectangles (a 3 × 2 square net), that is, a portion of an {001} B1 face. The straightening of these X–M–X–M... bonds in the B4 phase to the linear conformation in the B1 is responsible for the lengthening of the system cell in the b-direction and corresponding shortening in the a-direction, as illustrated by the bold arrows in the figure. The motion in the ab-plane is linked to a particular pattern of displacements perpendicular to this shown in figure 7(b) (also shown schematically in figure 7(c)). The boat configurations collapse to form '3 × 2' sections of B1 face perpendicular to the original B4 [ab]-plane. All of the anion–cation 'bonds' remain intact during this transition with the additional bond in the 3 × 2 face formed by the nearest-neighbour approach of the anion–cation pair originally at the bow and stern of the boat (that is, the original next-nearest-neighbour pair at separation Γ as shown in figure 1).

The crystallographic relationship between the two structures is relatively simple and, significantly, different to that between the B3 starting material and B1 end product. The $[0001]_{B4}$ direction transforms into the $[001]_{B1}$ whilst the $[10\bar{1}0]_{B4}$ becomes the $[100]_{B1}$, and the $[0100]_{B4}$ becomes the $[010]_{B1}$ as discussed previously [13]. As a result of these transformations, the direction of close-packed stacking (defined as the vector normal to the close-packed planes) has changed orientation.

5. B5 and SF → B1

The B5 polymorph has a stacking sequence ABACABAC... , i.e. the B5 unit cell sequence can be thought of as constructed from three hexagonally packed layers (ABA) with a further cubic-close-packed layer (C). Similarly, the SF structure is constructed from five hexagonal-packed layers (ABABA) linked to five alternately packed hexagonal layers (CBCBC) giving two stacking faults per cell; the regions around the stacking fault shift, however, could equally well be considered as a four-layer B3-like sequence (BACB). Given that the B3 and B4 structures appear to favour quite different pathways, it is interesting to see which pathway (if either) is preferred in systems which can be considered as a mixture of the two packing motifs. The intermediate nature of these two stacking sequences between the cubic-packed B3 structure and the hexagonal-packed B4 structure, is highlighted by the energy/ curves in figure 2 in which the en-

ergy minima of these two structure appear between those of the B3 and B4. Furthermore, table 1 shows the required driving pressures to be also intermediate between those for the B3 and B4.

Consider first the macroscopic properties. For the B5 → B1 transition, the a, b and c cell lengths change from 30.4, 30.4 and 19.6 au to 29.6, 41.9 and 17.1 au respectively (changes of −3, +38 and −13%). The $\widehat{ab}$ cell angle changes from 120° to 135° with the other two angles remaining unchanged. These changes are indicative of a B4 → B1-like transformation mechanism (figure 6).

Analogous comments again apply to the SF → B1 transformation. In this case the a, b and c cell lengths change from 30.3, 30.3 and 48.9 au to 29.4, 29.4 and 41.5 au respectively (−3, −3 and −15%) with the $\widehat{ab}$ cell angle changing from 120° to 90°. Again, these changes are fully consistent with the B4 → B1 transformation mechanism. The evolution of the 120° bond angle to 90° rather than to 135° is simply an equivalent distortion in the [ab]-plane to that shown in figure 7.

We can understand the preference for the B4 mechanism at a microscopic level by referring back to figure 5(b). The presence of the boat structures in the c-direction in the B4 structure does not allow for the formation of the same layers of distorted tetrahedra as in the B3 structure, and this will apply to the intermediate stackings as well, even though the 'concentration' of boats is lower. The compression of the tetrahedra is a relatively low-energy process but can only occur throughout the whole sample in the perfect B3 structure. To highlight this point, figure 8 shows the B5 structure prior to the phase transition. The layer highlighted by the arrow is between the AB and AC sections and is the only layer with the characteristic chair structure in the c-direction. As is clear from the figure, there is considerable strain on these bonds of the type observed in the B3 → B1 transition (figure 5(a) panel (ii)). However, since these units do not percolate across the structure, the transition cannot occur throughout the sample. The presence of the boat structure perpendicular to the ab-plane frustrates these tetrahedral compressions.

6. Comparison with experiment and *ab initio* calculation

Symmetry constraints on the possible pathways between B3, B4 and B1 structures have been considered by Sowa [2]. These general considerations underpin the discussion of the transition in different materials from a common standpoint. We considered the relationship between the B3 → B1 mechanism found in simulations for MCl and those proposed experimentally [18,19] in our previous paper [4]. For the B4 → B1 mechanism, the present work appears to support the mechanism discussed by Tolbert and Alivisatos [9] who consider the transformation in terms of the reverse (B1 → B4) pathway. In this mechanism, the transformation is dominated by the boat → 3 × 2 B1 face (the three-dimensional equivalent of the graphite → square net [20]) shown in figure 7. These motions are consistent with experimentally observed phonon mode and elastic constant softenings [21–23].

Experiments in which crystals of B4 CdS are shocked along both the a- and c-axes have been interpreted in terms of an intermediate (termed the face-centred tetragonal (fct) or face-centred orthorhombic (fco) structure—the latter is an orthorhombic distortion of the former). The pathway along which the ions move is, in fact, entirely consistent with the one observed here except that it is envisaged as proceeding in two stages. In the first, the basal ([ab]-) plane chairs (figure 1) collapse, just as in the MD simulation (figure 7(c), top panel), to form a five-coordinate structure (the fct) in which each ion is surrounded by a square-based pyramid of counter-ions, giving four equivalent (basal) bond lengths, and one unique length perpendicular to the basal plane. In the second step, the boats in the c-direction fold, as in figure 7(b) (hexagonal → square net), to form the 3 × 2-B1 face. The pattern of ion displacements seen in the simulations is exactly as in the proposed mechanism, but does not seem to take place

in two steps. The MD simulation does not, however, rule out the possibility of such a two-step transformation. The simulation work utilizes relatively small cells (although repeated infinitely) which may artificially favour such a concerted transformation mechanism, and the transformation occurs at a large overpressure which may drive the transition in a single step.

An apparently different mechanism has been proposed by Limpijumnong and Lambrecht [13, 14] who suggest a homogeneous shear strain deformation pathway linking the B4 and B1 structures. In this case, the suggested metastable intermediate structure (the h-MgO) can be thought of as derived from the B4 by compression along the c-axis only, that is, the second step in the above mechanism before the first. This proposed mechanism is equivalent to that incorporating the fct or fco intermediates but with the two steps reversed. The deformation can be characterized by the internal parameter u, which characterizes the distortion of the coordination tetrahedra and which varies from 0.375 in the ideal B4 to 0.5 in h-MgO. The result is that the ion coordination number rises to five with each ion surrounded by a trigonal biprism of counter-ions. *Ab initio* calculations suggest this as a metastable state for MgO, for which the B1 structure is energetically favourable over the B4 [14].

In order to investigate the potential stability of these proposed intermediates we have performed additional static energy minimizations on both the fct and h-MgO structures at a range of molar volumes, varying the c/a ratio in each case. These energy/volume curves are shown in figure 9 along with the B4 and B1 curves from figure 2. The energy minima are found for c/a ratios of 1.2 and 1.6 respectively. Both intermediates are found to be metastable with respect to the B1 and/or the B4 at all volumes (with the MCl potential). For the fct structure this is fully consistent with *ab initio* calculations (for CdS) [12] as is the predicted c/a ratio at the energy minimum.

Figure 9 also shows that the h-MgO structure is metastable with respect to the B1 and B4 at all volumes. Furthermore, the volume of the energy minimum actually moves to larger volume than that of the optimum B4 as the distortion of the tetrahedron (increasing u) tends to the ideal h-MgO structure. To highlight this point, the figure also shows the static energy/volume curve for the distortion intermediate between the B4 ($u = 0.375$) and h-MgO ($u = 0.5$) with $u = 0.45$.

With the MCl potential, the cation prefers to be four coordinate; that is, it is too small to efficiently fit into an octahedral hole. In the two intermediates the coordination number increase to five with respect to the B4 ground state, but with the formation of different ion geometries. In the fct, the square-based pyramid allows for a relatively efficient distribution of counter-ions about a given cation, so that the energy minimum occurs at a smaller volume than in the B4, but at a substantially higher energy. In the h-MgO, however, the trigonal equatorial grouping is relatively tightly held and so does not allow for the close approach of the additional two (axial) anions. As a result, this structure is best considered as $3+2$ coordinate, rather than five, and the idea that this is not a convenient arrangement for the MCl potential is consistent with the observed volume increase. This also results in the increased c/a ratio compared to that calculated *ab initio* for MgO [14] (1.6 compared with 1.2) and the two very different bond lengths (2.25 and 2.78 Åfor the equatorial and axial lengths respectively). However, we would expect that this structure would become more favourable for systems with comparatively large cations for which higher-coordinate geometries are stable. For MgO, the six-coordinate rocksalt structure is the lowest-energy structure, so the greater stability of the h-MgO structure for this system (compared with the MCl) is perhaps not surprising.

In summary, it would seem that the pathway followed by the ions in the mechanism of the B4 $\rightarrow$ B1 transition which we have observed in MCl is closely related to those which have been proposed in experimental studies of bulk crystals. This is in accord with Sowa's demonstration [2] that the pathway is constrained by the symmetries of the initial and final

phases. Apparent differences between mechanisms arise because of the relative stability of different intermediate coordination environments, which is affected by chemically specific features of the materials involved.

Wickham *et al* [3] discuss a further mechanism derived by fitting to x-ray diffraction patterns for the phase transition of small CdSe nanocrystallites (∼45 Å in diameter). The mechanisms derived here are not consistent with the observed shape changes in these crystallites. We would, however, anticipate that such small clusters may prefer alternative transition mechanisms to the bulk systems owing to the presence of significant surface energy effects. Furthermore, the observed transitions contain significant 'mixed' crystals with both B3 and B4 stacking sequences present. We shall consider the reverse transformation and the effect of crystal size and geometry elsewhere.

7. Conclusions

In this paper we have established atomistic transition mechanisms for the tetrahedral to octahedral B3 → B1 and B4 → B1 pressure-driven phase transformations for an MCI. By using constant-stress molecular dynamics, the dynamic transitions have been observed directly. Although closely related, and although the final crystal is the same in both cases, the B3 and B4 structures are found to transform via different mechanisms. The 'choice' of transformation mechanism is crucial in determining the crystallographic relationship between the starting material and the end product. The simulations have provided a means for understanding the relationship between a number of apparently different mechanisms which have been proposed for these transformations on the basis of experimental studies and helped to identify the chemical factors which determine which intermediate phases might play a role in different substances.

Our analysis indicates that the presence of the boatlike six-membered ring structures in the B4 phase are crucial in determining the choice of transformation mechanism. The idea that the presence of the boats frustrates a transition through a relatively low-energy pathway is supported at both a macro- and microscopic level. The systems studied which contain mixed hexagonal and cubic stacking sequences (contain stacking faults with respect to the idealized B3 and B4 crystals) are observed to transform via the B4 → B1 mechanism. The chairs in these systems are observed to undergo strains under isotropic compression very similar to those observed in the first step of the B3 → B1 mechanism (the tetrahedral compression). However, the boat structures prevent these distortions from percolating throughout the system and hence frustrate the concerted rearrangement required by this mechanism. Macroscopically, the energy associated with the overpressure required to drive the B3 → B1 transformation is significantly smaller than those associated with the other three studied systems, where boat structures are present. The frustration of the tetrahedral compression means that additional driving pressures are required to force the system to transform via the alternative mechanism.

Acknowledgment

MW thanks the Royal Society for a Research Fellowship.

Appendix—simulation conditions

To model the pressure-driven phase transitions, the system pressure is increased or decreased gradually in a well controlled fashion. The aim is to move slowly through the pressure range over which any transition may occur rather than to shock the system via a sudden pressure application. The external pressure is 'ramped' at pre-determined times by a pre-determined

Table A.1. Simulation cell sizes used in the present work. $n_a \times n_b \times n_c$ is the number of unit cells in each direction giving a total of $N_{molecules}$ molecules. The final column lists the ideal c/a ratios for each unit cell structure.

Structure	$n_a \times n_b \times n_c$	$N_{molecules}$	$(c/a)_{ideal}$
B4	$5 \times 5 \times 3$	150	$2\sqrt{2}/\sqrt{3}$
B3	$5 \times 5 \times 2$	150	$3\sqrt{2}/\sqrt{3}$
B5	$5 \times 5 \times 1$	100	$4\sqrt{2}/\sqrt{3}$
SF	$5 \times 5 \times 1$	250	$10\sqrt{2}/\sqrt{3}$

pressure increment, Δp, typically of the order of 10^{-4} au ($\equiv$3 GPa) every 10 000 time-steps ($\simeq$6 ps). This time period was found to be significantly longer than that required for the internal pressure to equilibrate about the new value. Of course, the transition should be completely unaffected by this change in boundary conditions. However, as Wentzcovitch pointed out, not all constant-stress MD algorithms are invariant to the choice of cell. The algorithm which we have employed, due to Martyna *et al* [16], should have this property.

Table A.1 lists the cells used in the present work along with the ideal c/a ratios for each structure. Simulations are performed at 300 K using a time step of 25 au ($\simeq$0.6 fs). Nosé–Hoover thermostats [24, 25] and barostats [16] are employed throughout with a thermostat relaxation time of 50 000 au and barostat parameters of 10 000 au. The effects of varying the barostat conditions have been considered previously in [4].

References

[1] Müller U 1993 *Inorganic Structural Chemistry* (Chichester: Wiley)
[2] Sowa H 2001 *Acta. Crystallogr. A* **57** 176
[3] Wickham J N, Herhold A B and Alivisatos A P 2000 *Phys. Rev. Lett.* **84** 923
[4] Wilson M, Hutchinson F and Madden P A 2002 *Phys. Rev.* B **65** 094109
[5] Hull S and Keen D A 1994 *Phys. Rev.* B **50** 5868
[6] Nelmes R J and McMahon M I 1998 *Semicond. Semimet.* **54** 145
[7] Pistorius C W F T 1976 *Prog. Solid State Chem.* **11** 1
[8] Ackland G J 2001 *Phys. Status Solidi* b **223** 361
[9] Tolbert S H and Alivisatos A P 1995 *J. Chem. Phys.* **102** 4642
[10] Tang Z P and Gupta Y M 1997 *J. Appl. Phys.* **81** 7203
[11] Sharma S M and Gupta Y M 1998 *Phys. Rev.* B **58** 5964
[12] Knudson M D, Gupta Y M and Kunz A B 1999 *Phys. Rev.* B **59** 11 704
[13] Limpijumnong S and Lambrecht W R L 2000 *Phys. Rev. Lett.* **86** 91
[14] Limpijumnong S and Lambrecht W R L 2001 *Phys. Rev.* B **63** 4103
[15] Chisholm J A and Bristowe P D 1999 *J. Phys.: Condens. Matter* **11** 5057
[16] Martyna G J, Tobias D J and Klein M L 1994 *J. Chem. Phys.* **101** 5
[17] Wentzcovitch R M 1991 *Phys. Rev.* B **44** 2358
[18] Keen D A and Hull S 1993 *J. Phys.: Condens. Matter* **5** 23
[19] Moore M J and Kasper J S 1968 *J. Chem. Phys.* **48** 2446
[20] Burdett J K and Lee S 1983 *J. Am. Chem. Soc.* **105** 1079
[21] Briggs R J and Ramdas A K 1976 *Phys. Rev.* B **13** 5518
[22] Mitra S S, Brafman O, Daniels W B and Crawford R K 1969 *Phys. Rev.* **186**
[23] Corll J A 1967 *Phys. Rev.* **157** 623
[24] Nosé S 1984 *J. Chem. Phys.* **81** 511
[25] Hoover W G 1985 *Phys. Rev.* A **31** 1695